nature chemical biology

ARTICLE

PUBLISHED ONLINE: 9 MAY 2016 | DOI: 10.1038/NCHEMBIO.2079

Global survey of cell death mechanisms reveals metabolic regulation of ferroptosis

Kenichi Shimada[1], Rachid Skouta[1,5], Anna Kaplan[1], Wan Seok Yang[1,5], Miki Hayano[2], Scott J Dixon[1,5], Lewis M Brown[3], Carlos A Valenzuela[5], Adam J Wolpaw[1,5] & Brent R Stockwell[1,4]*

Apoptosis is one type of programmed cell death. Increasingly, non-apoptotic cell death is recognized as being genetically controlled, or 'regulated'. However, the full extent and diversity of alternative cell death mechanisms remain uncharted. Here we surveyed the landscape of pharmacologically accessible cell death mechanisms. In an examination of 56 caspase-independent lethal compounds, modulatory profiling showed that 10 compounds induced three different types of regulated non-apoptotic cell death. Optimization of one of those ten resulted in the discovery of FIN56, a specific inducer of ferroptosis. Ferroptosis has been found to occur when the lipid-repair enzyme GPX4 is inhibited. FIN56 promoted degradation of GPX4. FIN56 also bound to and activated squalene synthase, an enzyme involved in isoprenoid biosynthesis, independent of GPX4 degradation. These discoveries show that dysregulation of lipid metabolism is associated with ferroptosis. This systematic approach is a means to discover and characterize novel cell death phenotypes.

Cells die not merely as a consequence of catastrophic failure of homeostasis, but also when regulated cell death is activated[1]. Apoptosis is a well-understood form of regulated cell death. The biological importance of apoptosis is highlighted by the fact that it is evolutionarily conserved in multicellular organisms[2], as well as by its use in developmental programs. The unique morphological and biochemical changes associated with apoptosis are due to the executioner caspase proteases. However, apoptosis is not the only form of regulated cell death. For example, cells commit to die after treatment with tumor necrosis factor-α, even when catalytic activity of the executioner caspase-3 is inhibited[3]. Intriguingly, non-apoptotic cell death can be blocked by small molecules; this is now appreciated as a type of regulated cell death, and has been implicated in several physiological contexts and pathological conditions[1,4,5]. Cells actively commit to die through non-apoptotic cell death in some physiological contexts, such as during infection: damage-associated and pathogen-associated molecular patterns are released from dying cells and trigger inflammatory responses of neighboring cells and immune cells[6].

Ferroptosis is a non-apoptotic form of regulated cell death. Numerous reports have demonstrated its relevance to pathological conditions, such as periventricular leukomalacia, nephrotic tubular death, and Huntington's disease[7,8]. Ferroptosis is distinct from other regulated cell death phenotypes, such as apoptosis and necroptosis[4,9]. Ferroptosis is characterized by extensive lipid peroxidation, which can be suppressed by iron chelators or lipophilic antioxidants. Ferroptosis inducers are divided into two mechanistic classes: (1) inhibitors of cystine import that act via system x_c^- (e.g., erastin, sorafenib, sulfasalazine and glutamate)[9,10], which subsequently cause depletion of glutathione (GSH)[11], and (2) direct, covalent inhibitors (e.g., (*1S*, *3R*)-RSL3) of glutathione peroxidase 4 (GPX4)[12]. Because GPX4 reduces lipid hydroperoxides using GSH as a cosubstrate[13], both compound classes ultimately result in loss of GPX4 activity followed by an increase in the amount of lipid reactive oxygen species (ROS) and consequent cell death.

There is some cross-talk among distinct regulated cell death phenotypes[4,14]. Generally each proposed cell death phenotype has been studied in a different model[15]. However, a universal comparison of different cell death phenotypes would be beneficial for improving understanding of the mechanisms governing cell death.

We hypothesized that evaluating diverse pharmacologically accessible cell death mechanisms would allow us to map the landscape of cell death. Among 3,169 compounds evaluated as cell death probes, we found 451 that were lethal without activating caspases. Of those, most activated unregulated necrotic death, but a technique known as modulatory profiling revealed that a subset of lethal compounds induced three types of regulated non-apoptotic cell death: metal-ion-dependent cell death, necrostatin-1-dependent cell death, and ferroptosis. Further optimization of one probe resulted in the discovery of FIN56, a new and specific inducer of ferroptosis. Ferroptosis has been reported to be induced when GPX4 is directly inhibited or indirectly inactivated by depletion of glutathione[12]. We found that, in contrast to these mechanisms, FIN56 induced ferroptosis by inducing degradation of GPX4. We performed a chemoproteomic analysis and found that FIN56 binds to and activates squalene synthase, an enzyme involved in cholesterol synthesis, to suppress non-steroidogenic metabolites—most likely coenzyme Q_{10}—in the mevalonate pathway, which enhances sensitivity to FIN56-induced ferroptosis. These discoveries together reveal that dysregulation of lipid metabolism is associated with ferroptosis.

RESULTS

Modulatory profiling revealed three kinds of cell death

To map the landscape of cell death, we sought small-molecule inducers of regulated, non-apoptotic cell death (**Fig. 1a**). We tested 3,169 lethal compounds for induction of caspase-independent cell death in HT-1080 fibrosarcoma cells and BJeLR engineered transformed fibroblasts, cell lines used previously for modulatory profiling experiments[16] (**Supplementary Results**, **Supplementary Table 1**).

[1]Department of Biological Sciences, Columbia University, New York, New York, USA. [2]Department of Pharmacology, Columbia University, New York, New York, USA. [3]Quantitative Proteomics Center, Columbia University, New York, New York, USA. [4]Department of Chemistry, Columbia University, New York, New York, USA. [5]Present addresses: Department of Chemistry, Border Biomedical Research Center, the University of Texas at El Paso, El Paso, Texas, USA (R.S. and C.A.V.); Department of Biological Sciences, St. John's University, Queens, New York, USA (W.S.Y.); Department of Biology, Stanford University, Stanford, California, USA (S.J.D.); Divisions of Hematology and Oncology, the Children's Hospital of Philadelphia, Philadelphia, Pennsylvania, USA (A.J.W.). *e-mail: bstockwell@columbia.edu

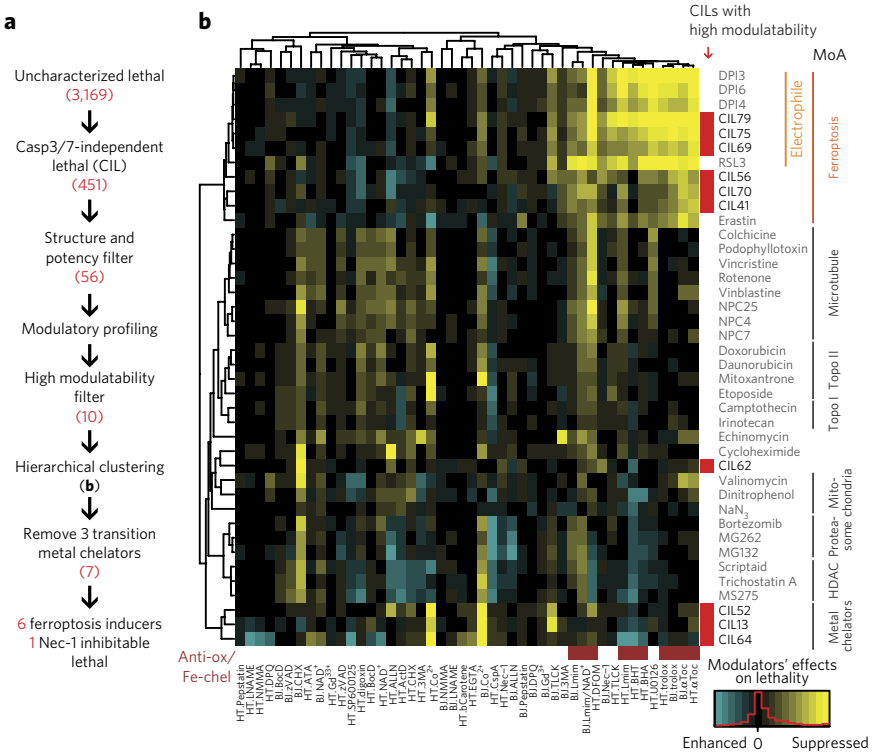

Figure 1 | Modulatory profiling revealed three types of regulated non-apoptotic cell death. (**a**) Experimental scheme to identify regulated non-apoptotic cell death inducers with high modulatability. The numbers in red indicate the number of compounds satisfying each criterion. (**b**) Hierarchical clustering of modulatory profiles of 10 CILs with high modulatability and 30 characterized lethal compounds from several classes of lethal mechanisms. Lethal compounds are listed on the right. Ten CILs are indicated by red shading. Forty-six modulators are listed along the bottom (28 death modulators in two cell lines, HT-1080 and BJeLR). Antioxidants (anti-ox) and iron chelators (Fe-chel) are indicated by brown shading. MoA, mechanism of action; Topo, topoisomerase. A detailed list of modulators is shown in **Supplementary Table 2**. **Supplementary Figures 1–4** show additional data on the CIL screening scheme, the modulatory profiling scheme, and structures and characterization of ten regulated non-apoptotic cell death inducers.

We found that 451 compounds (14%) triggered cell death without activation of caspases 3 and 7, detected using a fluorogenic substrate. These compounds were defined as 'caspase-3/7-independent lethals' (CILs) (**Supplementary Fig. 1** and **Supplementary Note 1**). Thus, although most lethal compounds activate caspase activity (irrespective of whether caspase activity is required for their lethality), we found that a considerable number of compounds were lethal without activating cleavage of the fluorogenic caspase-activity probe.

We examined in more detail 56 structurally diverse and potent (EC_{80} < 2.8 μg ml^{-1}) CILs using a modulatory profiling strategy. In a previous study, the clustering of modulatory profiles, or changes in the potency and efficacy of a lethal compound induced by cotreatment with chemical and genetic death modulators (**Supplementary Table 2**), revealed that compounds with the same mechanism of action share similar modulatory profiles[17]. For evaluation of diverse regulated cell death programs, modulatory profiling should facilitate the grouping of pharmacological agents by their induction of specific regulated cell death programs. We observed ten compounds that induced three types of regulated non-apoptotic cell death. We further identified a specific ferroptosis inducer through lead optimization and uncovered its mechanism of action. In this analysis, 10 of the 56 CIL compounds exhibited 'high modulatability', meaning their lethality was considerably suppressed or enhanced by specific pharmacological or genetic agents[17] (**Supplementary Fig. 2** and **Supplementary Data Set 1**); high modulatability correlates with activity through a specific lethal pathway. When analyzed along with other well-characterized lethal compounds, these CILs fell into three classes (**Fig. 1b** and **Supplementary Fig. 3a**). The first class (CIL13, CIL52, and CIL64) acted via metal chelation, as these compounds were inhibited by cobalt (II) and bound to cobalt (II) *in vitro* (**Supplementary Fig. 3b,c**). The second class (CIL62) induced cell death that was suppressed by necrostatin-1 (ref. 18) (**Supplementary Fig. 3d,e**; note that this does not necessarily imply necroptosis, as necrostatin-1 has necroptosis-independent effects[19]), and the third class (CIL41, CIL56 (**1**), CIL69, CIL70, CIL75, and CIL79) comprised ferroptosis inducers, as suggested by their suppression by canonical ferroptosis inhibitors (iron chelators and lipophilic antioxidants; **Supplementary Table 3**) and clustering with known ferroptosis inducers. We focused further studies on the six CIL compounds that clustered with ferroptosis inducers.

Of the six ferroptotic CILs, three (CIL69, CIL75, and CIL79) are putative electrophiles and clustered most closely with known electrophilic ferroptosis inducers, such as (*1S*, *3R*)-RSL3 (**Supplementary Fig. 4a**). The remaining CILs consisted of two novel scaffolds: CIL41/70 and CIL56. CIL41/70 induced ROS accumulation, detected using H_2-DCFDA (**Supplementary Fig. 4b**), and cell death that was strongly suppressed by ferroptosis inhibitors (i.e., the lipophilic antioxidant α-tocopherol and the iron chelator deferoxamine) (**Supplementary Fig. 4c**).

All known ferroptosis inducers induce selective lethality in a BJ engineered cell line series, namely, BJeH, BJeHLT, DRD, and BJeLR cells. These cells were initially created to demonstrate that normal human fibroblasts can be transformed into tumor cells by the introduction of defined genetic elements (human telomerase, SV40 small and large T antigens, and oncogenic *HRAS*^{G12V})[16]. BJeLR cells and DRD cells, which overexpress oncogenic RAS, were found to be more sensitive to ferroptosis inducers than BJeHLT cells and BJeH cells, which do not express oncogenic RAS. CIL41/70, unlike all other ferroptosis-inducing compounds reported to date, did not exhibit oncogenic *RAS* selectivity in the BJ engineered cell line series[20] (**Supplementary Fig. 4d**). Moreover, we tested 203 commercially available structural analogs of CIL41/70 and found them to be less potent than CIL56 itself (**Supplementary Note 1** and **Supplementary Fig. 4e**). Given that CIL56 was the most potent compound, and that it retained some degree of selectivity toward oncogenic-*RAS*-expressing cells in the BJ series (**Fig. 2a**), we speculated that CIL56 was more likely than CIL41/70 to yield a potent and selective probe of ferroptosis. Thus, we selected CIL56 for more detailed characterization.

Probe optimization led to a specific ferroptosis inducer

CIL56 induced iron-dependent ROS (**Fig. 2b**). Antioxidants and iron chelators suppressed the lethality of low concentrations of CIL56 (**Fig. 2c**). We thus hypothesized that CIL56 was capable of engaging two independent death pathways: ferroptosis at low concentrations, and necrotic, non-suppressible cell death at higher concentrations. We sought to identify a more selective analog of CIL56 that retained the ability to induce ferroptosis but lacked the ability to induce the other form of death. Structure–activity

relationship analysis of the CIL56 scaffold determined that the oxime moiety was crucial for inducing ferroptosis, and that hydrophobicity of the piperidine moieties of CIL56 correlated with potency (**Supplementary Fig. 5**). Ultimately, we discovered an analog (SRS7-34) that has cyclohexylamine moieties in place of the piperidine moieties of CIL56 (**Fig. 2d**). This new compound, termed FIN56 (**2**) (ferroptosis inducer derived from CIL56), exhibited greater potency as well as greater oncogenic *RAS* selectivity in the BJ cell line series compared to CIL56 (**Fig. 2e**); FIN56 was also fully suppressed by the ferroptosis inhibitors deferoxamine and α-tocopherol (**Fig. 2f**), indicating that it engages only ferroptosis and does not have the ability to engage the second death mechanism activated by CIL56.

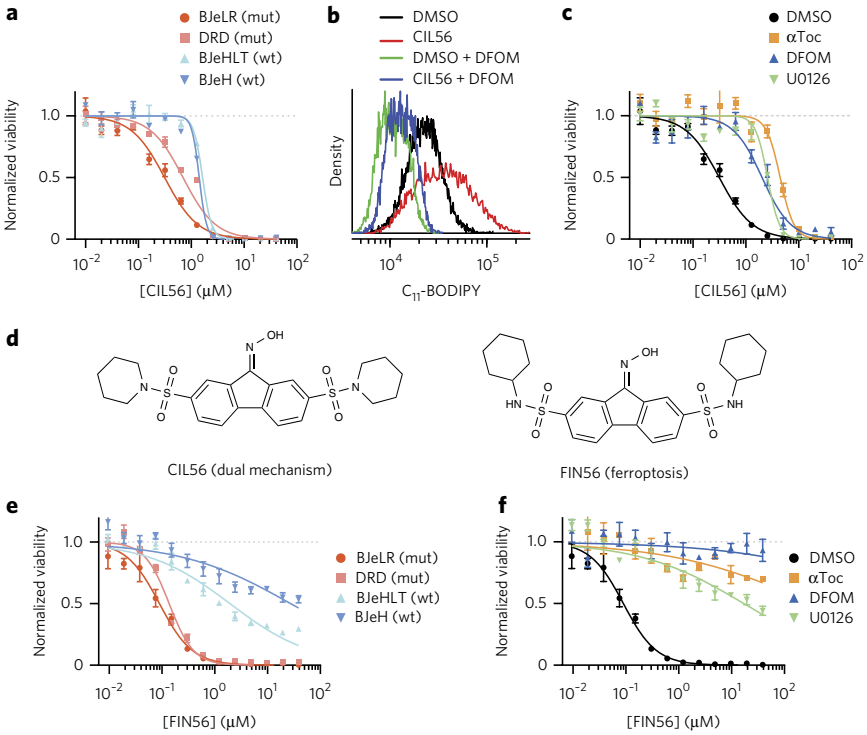

Figure 2 | Optimization of CIL56 revealed a potent and selective ferroptosis inducer. (**a**,**e**) *HRAS*^{G12V} selectivity. Viability of four engineered BJ cell lines treated with (**a**) CIL56 or (**e**) FIN56 for 48 h. mut, cells tumor-transformed as a result of *HRAS*^{G12V} overexpression; wt, isogenic cells without *HRAS*^{G12V}. (**b**) Lipid ROS generation. Flow cytometry analysis with BODIPY-581/591 C_{11} staining in HT-1080 cells incubated with test compounds for 6 h. DFOM, 152 μM deferoxamine. (**c**,**f**) Effects of ferroptosis inhibitors on viability of HT-1080 cells cotreated with (**c**) CIL56 or (**f**) FIN56 for 48 h. αToc, 100 μM α-tocopherol; U0126 was applied at 3.8 μM. (**d**) Chemical structures of CIL56 and FIN56. See **Supplementary Figure 5** for the structure–activity relationship around the CIL56 scaffold. Experiments for **a**–**f** were performed in biological triplicate, and data are presented as mean ± s.e.m. of technical triplicates.

FIN56-induced ferroptosis involves decreased GPX4 abundance

Previously reported ferroptosis inducers either deplete glutathione (by inhibiting cystine uptake) or are covalent GPX4 inhibitors. In the NCI60 cell line panel[21], we found that GPX4 inhibitors were more cell-line selective than compounds inducing glutathione depletion[22] (**Supplementary Fig. 6a**). In this regard, FIN56 was more similar to other GPX4 inhibitors than to GSH-depleting compounds. Supporting this, we found that FIN56 did not deplete glutathione, which suggested that it also did not block cystine import; however, FIN56 did cause the loss of GPX4 activity in cell lysates (**Fig. 3a** and **Supplementary Fig. 6b**). Intriguingly, compared to the covalent GPX4 inhibitor (*1S*, *3R*)-RSL3, FIN56 was slower to induce the accumulation of ROS (**Fig. 3b**), which suggested that it did not cause a loss of GPX4 activity via direct inhibition of enzymatic activity. Indeed, we determined that the abundance of GPX4, but not that of the related selenoprotein GPX1, was substantially decreased after FIN56 treatment (5 μM, 10 h) (**Fig. 3c** and **Supplementary Fig. 6c**,**d**). Neither erastin nor (*1S*, *3R*)-RSL3 affected the abundance of GPX4 to the same extent as FIN56, demonstrating that this effect was specific to FIN56. GPX4 knockdown enhanced FIN56 lethality (**Fig. 3d**), and FIN56-induced cell death was suppressed by GFP–GPX4 fusion-protein overexpression (**Fig. 3e**,**f** and **Supplementary Fig. 6e**,**f**), suggesting that the loss of GPX4 was critical for FIN56-induced ferroptosis. We also confirmed that selenite supplementation, which is known to upregulate the expression of selenoproteins, including GPX4 (ref. 23), also suppressed FIN56 lethality (**Supplementary Fig. 6g**,**h**). The decrease in GPX4 protein abundance was not inhibited by α-tocopherol, indicating that it was not a downstream consequence of lipid ROS generation. Together, these results suggested that FIN56 triggers ferroptosis through a mechanism involving the downregulation of GPX4 protein abundance.

We further investigated how FIN56 causes a decrease in the amount of GPX4 protein. We found that the *GPX4* transcript level increased, rather than decreased, after FIN56 treatment (**Supplementary Fig. 6i**), which suggests that FIN56-induced depletion of GPX4 protein is not mediated by transcriptional changes in *GPX4* mRNA. Observations that cells treated with cycloheximide, which inhibits ribosome function, did not show substantially decreased amounts of GPX4 protein compared to a housekeeping α-tubulin protein (**Supplementary Fig. 6j**) and that knockdown of the gene tRNA isopentenyltransferase 1 (*TRIT1*)[24], which has been reported to be required for synthesis of selenoproteins, including of GPX4, did not dramatically affect GPX4 protein abundance (**Supplementary Fig. 6k–m**) suggested that FIN56 did not inhibit GPX4 protein synthesis but rather induced post-translational GPX4 protein degradation. It is not clear, however, how GPX4 degradation is regulated, because a proteosome inhibitor (MG132) did not inhibit GPX4 degradation significantly or protect cells from FIN56 lethality. It is of note that GPX4 abundance was reported to decrease when the proto-oncogene serine/threonine-protein (Pim) kinases were inhibited[25]; however, this is not relevant to FIN56 lethality because pan-Pim kinase inhibitors did not induce ferroptosis, as these compounds were not suppressed by α-tocopherol (**Supplementary Fig. 6n**).

SQS encoded by *FDFT1* is a target protein of FIN56

To better understand the mechanism of action of FIN56, we sought proteins binding directly to FIN56 using a chemoproteomic approach. First, we explored structural analogs of FIN56. This resulted in the creation of SRS11-31, an analog with a polyethylene glycol (PEG) moiety, which induces ferroptosis at tenfold higher EC_{50} than FIN56 (**Fig. 4a** and **Supplementary Fig. 7**). In contrast, substitution of the cyclohexyl moiety in FIN56 with a 4-tetrahydropyran (SRS8-18 (**3**)) or its PEG conjugate (SRS11-66) (**4**) resulted in a complete loss of activity. Next, we conjugated both SRS11-31 (**5**) (active, or A) and SRS11-66 (inactive, or I) to Profinity epoxide resin via an epoxy ring-opening reaction and incubated the resins with HT-1080 whole-cell lysates. We used mass spectrometry to

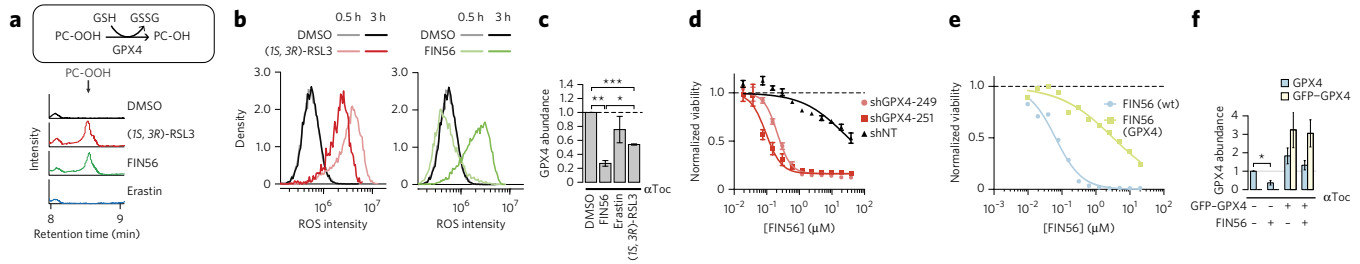

Figure 3 | FIN56-induced ferroptosis decreases GPX4 expression. (**a**) GPX4 enzymatic activity in BJeLR cells after ferroptosis-inducer treatment. GSSG, oxidized glutathione; PC, phosphatidylcholine. (**b**) Kinetics of ROS generation after treatment with 0.5 μM (*1S*, *3R*)-RSL3 or 5 μM FIN56, detected with 25 μM H_2-DCFDA staining in BJeLR cells. (**c**) GPX4 protein abundance in BJeLR cells after cotreatment with 100 μM α-tocopherol and ferroptosis inducers for 10 h. (**d**) The effect of shRNA targeting *GPX4* (shGPX4) on FIN56-induced ferroptosis in BJeLR cells. shNT, nontargeting shRNA. (**e**) The effects of GFP–GPX4 fusion-protein overexpression on sensitivity to FIN56 in BJeLR cells. (**f**) The effects of GFP–GPX4 fusion-protein overexpression on endogenous and exogenous GPX4 protein abundance after FIN56 treatment. **Supplementary Figure 6** supports the connection between FIN56 and GPX4 and shows western blots corresponding to **c** and **f**. $^*P < 0.05$, $^{**}P < 0.005$, $^{***}P < 0.0005$ (paired two-tailed *t*-test). Experiments in **a**–**f** were done in biological triplicate. Representative results are shown for **a**, **b** and **e**; data in **c** and **f** are the mean ± s.e.m. of biological triplicates; data in **d** are the mean ± s.e.m. of technical triplicates.

identify and quantify the pulldown proteins found with each probe. Seventy proteins, excluding universally expressed proteins (actins, tubulins, and ribosome subunits), were found to be more abundant on the resin conjugated with the active probe.

We tested whether these candidate target proteins were inhibited (loss of function) or activated (gain of function) by FIN56 to induce ferroptosis using RNA interference (RNAi). RNAi-mediated knockdown of the relevant target should either enhance or suppress FIN56 sensitivity, depending on FIN56's mechanism of action (**Supplementary Fig. 8a**). Expression of many genes is affected by off-target effects of RNAi, and the resulting phenotypes may differ from cell line to cell line; however, on-target effects are more likely to be consistent among different cell lines. Therefore, we examined the effects of up to five short hairpin RNA (shRNA) clones per gene encoding 70 candidate target proteins in four independent ferroptosis-susceptible cell lines: HT-1080, BJeLR, Calu-1 lung adenocarcinoma, and 143B osteosarcoma (**Fig. 4b** and **Supplementary Fig. 8b**,**c**). We sought candidate FIN56 targets responsible for ferroptosis using two criteria: (i) high selective abundance on the active versus inactive probe resins, and (ii) high proportion of consistently performing shRNAs in all four cell lines subjected to RNAi-mediated silencing of each gene (**Fig. 4c**

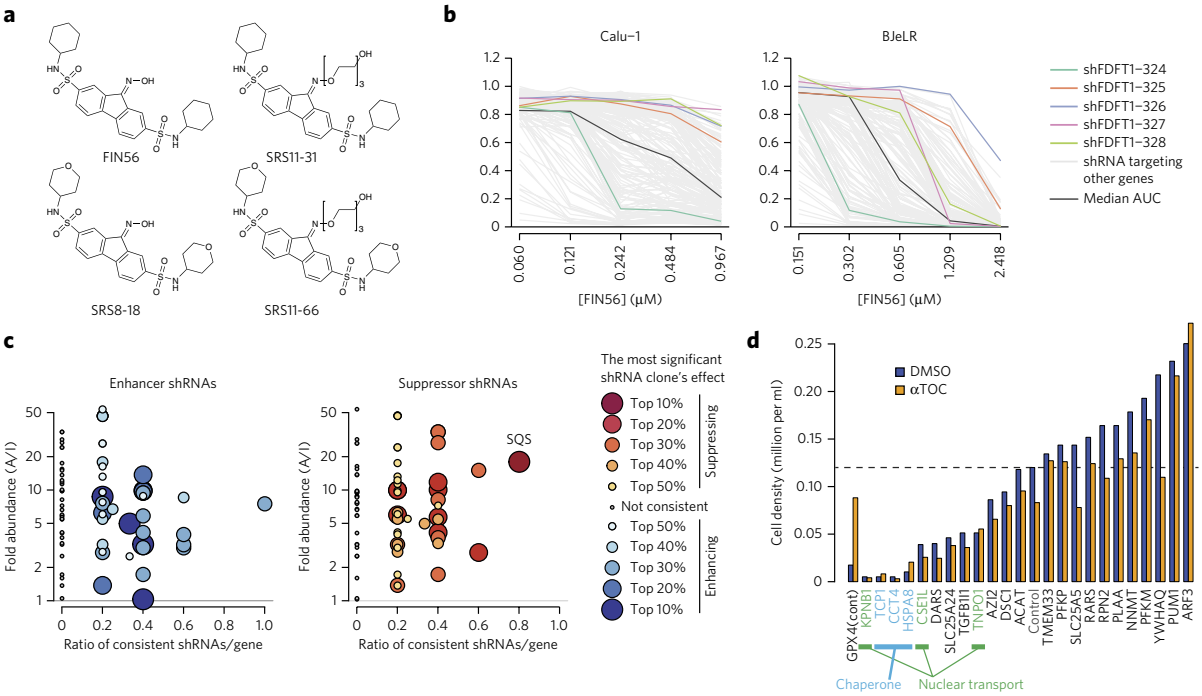

Figure 4 | SQS encoded by *FDFT1* as FIN56's target protein. (**a**) Active and inactive FIN56 analogs with PEG linkers. **Supplementary Figure 7** shows their potency in HT-1080 cells. (**b**) Effects of five shRNAs against *FDFT1* on FIN56. Results in two of the four cell lines are shown. The black line in each graph (median AUC among tested shRNAs) represents a shRNA that had no effect in each cell line. (**c**) Summary of proteomic target identification and effect of shRNA screening targeting 70 identified genes on FIN56. Each dot summarizes the result of multiple shRNAs targeting a gene. Each shRNA was considered 'consistent' when it exerted the indicated effect (enhancing or suppressing FIN56). *X*-axis represents the ratio of the number of consistent shRNAs inducing the indicated effect (i.e., enhancing or suppressing FIN56) to the total number of shRNAs targeting the gene. *Y*-axis shows fold enrichment of protein abundance on active versus inactive probe beads in a pulldown assay. See **Supplementary Figure 8** for more details. (**d**) Effect of siRNAs against loss-of-function candidates on BJeLR cell viability. Cells were grown in the presence of DMSO or α-tocopherol. shRNA screens in **b**,**c** were performed once in four cell lines. The siRNA experiment in **d** was performed in BJeLR twice, and results indicate the mean of biological replicates.

and **Supplementary Fig. 8d**). Among the 70 tested proteins, we found proteins, such as chaperones and nuclear transport proteins, for which knockdown not only enhanced FIN56 lethality but also independently induced toxicity. However, their lethality was not suppressed by α-tocopherol, unlike with GPX4 knockdown, indicating that these cell death phenotypes were distinct from ferroptosis. The potency of FIN56 might be aided by modulation of these essential proteins, but they are not the primary targets of FIN56 (**Fig. 4d**).

Validating the functional relevance of the target

We found that four of the five shRNAs against *FDFT1* mRNA (which encodes SQS protein) suppressed FIN56 consistently in all four cell lines tested, indicating that FIN56 activates, rather than inhibits, SQS (a gain-of-function model). Therefore, we explored this possibility and studied how the FIN56–SQS interaction is relevant to FIN56's lethality. We confirmed that not only shRNAs targeting *FDFT1* but also small-molecule inhibitors of SQS activity (YM-53601 and zaragozic acid A) suppressed FIN56 lethality (**Fig. 5a**). SQS is an enzyme that acts downstream of 3-hydroxy-3-methylglutaryl-coenzyme A (HMG-CoA) reductase in the mevalonate pathway. SQS couples two farnesyl pyrophosphate (FPP) molecules to form squalene. Inhibition of SQS consequently increases the pool of FPP. FPP is essential for several processes, including protein prenylation and metabolite synthesis (e.g., sterols, coenzyme Q_{10} (CoQ_{10}), dolichol, and heme)[26], some subset of which may be relevant to the modulatory effect on ferroptosis sensitivity. Supplementation with FPP indeed suppressed the lethality of FIN56 (**Fig. 5b**). We also examined SQS–FIN56 binding by confirming that SQS from HT-1080 whole-cell lysate bound selectively to active probes versus to an inactive probe (**Fig. 5c**). Moreover, bacterially expressed truncated human SQS protein[27] (with the lipophilic N and C termini removed) binding to an active affinity probe was efficiently suppressed by pre-incubation of purified SQS protein with FIN56, suggesting that SQS and FIN56 directly interact (**Supplementary Fig. 9**).

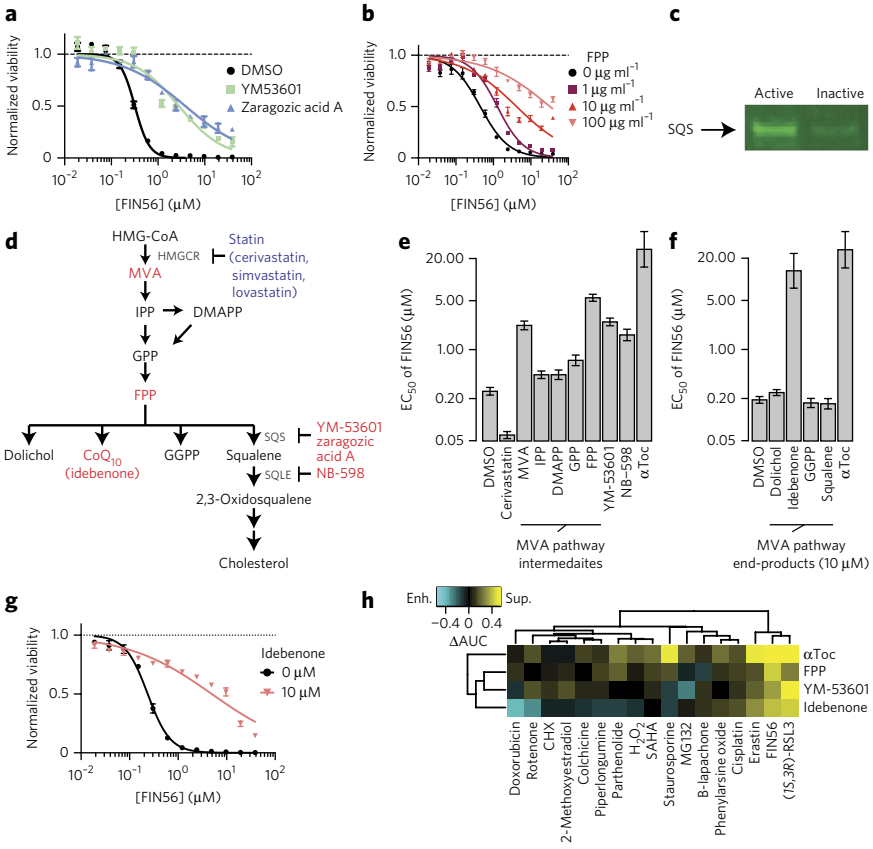

Figure 5 | Validating SQS as the functionally relevant target for FIN56's lethality. (**a**) Effects of chemical inhibitors of SQS on FIN56's lethality. (**b**) Effects of FPP on FIN56's lethality. (**c**) Detection of SQS via pulldown assay from HT-1080 whole-cell lysate with active or inactive probes. Note that the probes are the same as those used for chemoproteomic target identification. (**d**) Schematic of the mevalonate pathway. The larger font indicates metabolites, and the smaller font indicates enzymes responsible for the reactions or small molecules. Red or blue text indicates molecules (inhibitors or metabolites) that suppressed or enhanced FIN56's lethality, respectively. The detailed results are shown in **e** and **f**. (**e**) Perturbation of the mevalonate pathway and effects on FIN56's lethality. Concentrations: cerivastatin, 1 μM; metabolites, 100 μM; YM-53601, 5 μM; NB-598, 25 μM; α-tocopherol, 100 μM. (**f**) Supplementation of 10 μM end-products of the MVA pathway and their effects on FIN56. (**g**) Effect of 10 μM idebenone on FIN56 in HT-1080 cells. (**h**) Modulatory profiling between the modulators of the MVA pathway and various lethal compounds inducing oxidative stress. Enh., enhancement; sup., suppression; IPP, isopentenyl-pyrophosphate (PP); DMAPP, dimethylallyl-PP; GPP, geranyl-PP; FPP, farnesyl-PP; GGPP, geranylgeranyl-PP. See **Supplementary Figures 9** and **10** for SQS pulldown with competition and effect of statins on FIN56 lethality. **a**,**b**,**g** were performed in biological replicates, and data are presented as mean ± s.e.m. of technical triplicates; **e**,**f** were performed in biological duplicates, and data are presented as mean ± s.e. of EC_{50} estimation from sigmoidal curve-fitting; **h** was performed in singlicate. Effects of mevalonate pathway modulators without FIN56 on viability are presented in **Supplementary Figure 13**. The full image from **c** is presented in **Supplementary Figure 14**.

We focused on the role of processes upstream of FPP in the mevalonate pathway. We found that statins, chemical inhibitors of HMG-CoA reductase, enhanced FIN56 lethality (**Supplementary Fig. 10a**). HMG-CoA reductase synthesizes mevalonic acid (MVA). Supplementation of MVA reversed the effect of cerivastatin, the most potent and selective statin tested (**Supplementary Fig. 10b**,**c**), demonstrating that the HMG-CoA-reductase-inhibiting effect of cerivastatin is responsible for its enhancement of FIN56 lethality. However, we also realized that these effects did not affect GPX4 abundance (**Supplementary Fig. 10d**).

More extensive investigation of the mevalonate pathway showed that supplementation of FPP suppressed FIN56 more effectively than treatment with other isoprenoid pyrophosphates did, which suggests that FPP is functionally relevant to the regulation of sensitivity to FIN56 (**Fig. 5d**). We also found that an inhibitor of squalene monooxygenase, which is involved in a rate-limiting step downstream of SQS in cholesterol synthesis[28], and an SQS inhibitor both suppressed FIN56 lethality, supporting the notion that non-steroidogenic products of the mevalonate pathway contribute to the suppression of FIN56 (**Fig. 5e**). We found that among the metabolites derived from FPP, idebenone, a hydrophilic analog of CoQ_{10}, was the only suppressor of FIN56-induced ferroptosis (**Fig. 5f**,**g**), which suggests that CoQ_{10} mediates the connection between the mevalonate pathway and regulation of sensitivity to FIN56. Note that supplementation of CoQ_{10} itself is known to be ineffective because of its extreme hydrophobicity[29]. To further assess the specificity of the three mevalonate-pathway modulators (FPP, YM-53601, and idebenone), and of α-tocopherol, we used

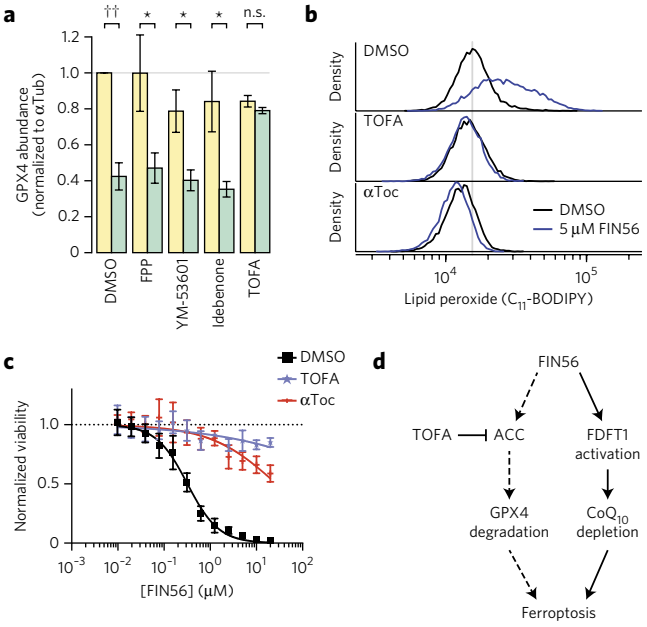

Figure 6 | ACC inhibitor prevents GPX4 protein degradation. (**a**) Effects of mevalonate pathway modulators and ACC inhibitor on GPX4 abundance with 0.1% DMSO (green) or 5 μM FIN56 (yellow). The corresponding gel is shown in **Supplementary Figure 12**. αTub, α-tubulin. $^{*}P < 0.05$, $^{\dagger\dagger}P < 0.001$ (paired two-tailed *t*-test); n.s., not significant. Modulator concentrations: DMSO, 0.1%; FPP, 10 μM; YM-53601, 5 μM; idebenone, 10 μM; TOFA, 10 μM. (**b**) Lipid peroxide levels after treatment with DMSO, TOFA or α-tocopherol. (**c**) Effects of TOFA and α-tocopherol on FIN56 lethality. (**d**) Model of FIN56's mechanism of action. Dashed arrows indicate that the mechanistic details are still elusive. **Supplementary Figure 11d** also supports the finding that the mevalonate pathway modulators did not change GPX4 abundance. Experiments for **a**–**c** were performed in biological triplicates. Data in **a** and **c** are presented as the mean ± s.e.m. of triplicates; single representative results are shown in **b**.

a modulatory profiling scheme in HT-1080 cells with lethal compounds, including ones that induce oxidative stress. We found that both GPX4 inhibitors, FIN56 and (*1S*, *3R*)-RSL3, were potently suppressed by all the compounds (**Fig. 5h**). Erastin, a GSH depletor, was also suppressed somewhat by the modulators; the rest of the compounds showed more distinct patterns. These results suggest that modulators of the mevalonate pathway are specific inhibitors of ferroptosis, rather than of lethality in general.

CoQ_{10} is an electron carrier in the mitochondrial respiratory chain and an endogenous antioxidant. However, whether it functions in the regulation of ferroptosis via either of these mechanisms remains to be elucidated. 143B cells with or without mitochondrial DNA (ρ^+ or ρ^0 cells, respectively) were both sensitive to FIN56-induced ferroptosis (**Supplementary Fig. 11a**,**b**), which suggests that the respiratory chain is not involved in ferroptosis. The lipophilic antioxidant α-tocopherol suppressed staurosporine-induced cell death, but idebenone enhanced it, suggesting that idebenone has distinct antioxidant properties compared to α-tocopherol. In addition, although both α-tocopherol and idebenone inhibited lipid ROS generation after FIN56 treatment, idebenone treatment did not change the basal lipid ROS level (**Supplementary Fig. 11c**). Thus, exactly how CoQ_{10} protects cells from FIN56 remains elusive, but the process may involve reprogramming of lipid metabolism in a way that is not conducive to the execution of ferroptosis, or a specific antioxidant action distinct from that of α-tocopherol.

An ACC inhibitor prevents GPX4 protein degradation

Modulators of the mevalonate pathway, such as idebenone, are potent suppressors of ferroptosis, particularly of direct and indirect GPX4 inhibitors (FIN56 and (*1S*, *3R*)-RSL3) (**Fig. 5h**); however, these compounds did not block the decrease in GPX4 protein abundance caused by FIN56 treatment or induce overexpression of the protein (**Fig. 6a** and **Supplementary Fig. 12**), indicating that there may be an additional pathway that regulates GPX4 protein level in response to FIN56 treatment. We discovered that 5-(tetradecyloxy)-2-furoic acid (TOFA), an inhibitor of acetyl-CoA carboxylase (ACC), inhibited the loss of GPX4. TOFA was also found to be a potent suppressor of FIN56 and suppressed lipid ROS generation after FIN56 treatment (**Fig. 6b**,**c**). ACC is an enzyme involved in fatty acid synthesis. We previously observed through genetic screening that ACC's activity is involved in the mechanism of non-ferroptotic cell death induced by CIL56 (ref. 30). However, ACC itself was not identified as a direct FIN56 target, and the detailed mechanism linking FIN56 to ACC remains to be understood.

In conclusion, characterization of FIN56 revealed that its mechanism involves two distinct pathways (**Fig. 6d**): degradation of GPX4, which requires the enzymatic activity of ACC; and activation of SQS, which leads to coenzyme Q_{10} depletion. Together these effects result in potent induction of ferroptosis.

DISCUSSION

Ferroptosis inducers were initially discovered through screens for oncogenic *RAS* synthetic lethality in BJ engineered cells. It might not be a coincidence that $HRAS^{G12V}$ not only induces malignant transformation but also sensitizes cells to ferroptosis inducers in the cells, as overexpression of oncogenic Ras is reported to modulate lipid metabolism[31–33]. Indeed, our studies suggest that fatty acid synthesis and the mevalonate pathway both regulate sensitivity to ferroptosis through distinct mechanisms. These and other studies of regulated non-apoptotic cell death and of its intersection with lipid metabolism are still at an early stage.

This systematic discovery and characterization of different cell death phenotypes has suggested that ferroptosis is an important form of pharmacologically accessible cell death. In the future, pharmacological cell death stimuli examined with modulatory profiling may reveal additional cell death mechanisms[22]. The inventory of regulated cell death discovered via these systematic approaches may provide insight into a global view of the possibilities of cell death.

Received 13 March 2015; accepted 15 March 2016;
published online 9 May 2016

METHODS

Methods and any associated references are available in the online version of the paper.

References

1. Fuchs, Y. & Steller, H. Programmed cell death in animal development and disease. *Cell* **147**, 742–758 (2011).
2. Aravind, L., Dixit, V.M. & Koonin, E.V. The domains of death: evolution of the apoptosis machinery. *Trends Biochem. Sci.* **24**, 47–53 (1999).
3. Degterev, A. *et al.* Identification of RIP1 kinase as a specific cellular target of necrostatins. *Nat. Chem. Biol.* **4**, 313–321 (2008).
4. Vanden Berghe, T., Linkermann, A., Jouan-Lanhouet, S., Walczak, H. & Vandenabeele, P. Regulated necrosis: the expanding network of non-apoptotic cell death pathways. *Nat. Rev. Mol. Cell Biol.* **15**, 135–147 (2014).
5. Kaczmarek, A., Vandenabeele, P. & Krysko, D.V. Necroptosis: the release of damage-associated molecular patterns and its physiological relevance. *Immunity* **38**, 209–223 (2013).
6. Kono, H. & Rock, K.L. How dying cells alert the immune system to danger. *Nat. Rev. Immunol.* **8**, 279–289 (2008).
7. Skouta, R. *et al.* Ferrostatins inhibit oxidative lipid damage and cell death in diverse disease models. *J. Am. Chem. Soc.* **136**, 4551–4556 (2014).
8. Linkermann, A. *et al.* Synchronized renal tubular cell death involves ferroptosis. *Proc. Natl. Acad. Sci. USA* **111**, 16836–16841 (2014).
9. Dixon, S.J. *et al.* Ferroptosis: an iron-dependent form of nonapoptotic cell death. *Cell* **149**, 1060–1072 (2012).

10. Dixon, S.J. *et al.* Pharmacological inhibition of cystine-glutamate exchange induces endoplasmic reticulum stress and ferroptosis. *eLife* **3**, e02523 (2014).
11. Hayano, M., Yang, W.S., Corn, C.K., Pagano, N.C. & Stockwell, B.R. Loss of cysteinyl-tRNA synthetase (CARS) induces the transsulfuration pathway and inhibits ferroptosis induced by cystine deprivation. *Cell Death Differ.* **23**, 270–278 (2016).
12. Yang, W.S. *et al.* Regulation of ferroptotic cancer cell death by GPX4. *Cell* **156**, 317–331 (2014).
13. Imai, H. & Nakagawa, Y. Biological significance of phospholipid hydroperoxide glutathione peroxidase (PHGPx, GPx4) in mammalian cells. *Free Radic. Biol. Med.* **34**, 145–169 (2003).
14. Linkermann, A., Stockwell, B.R., Krautwald, S. & Anders, H.-J. Regulated cell death and inflammation: an auto-amplification loop causes organ failure. *Nat. Rev. Immunol.* **14**, 759–767 (2014).
15. Hitomi, J. *et al.* Identification of a molecular signaling network that regulates a cellular necrotic cell death pathway. *Cell* **135**, 1311–1323 (2008).
16. Hahn, W.C. *et al.* Creation of human tumour cells with defined genetic elements. *Nature* **400**, 464–468 (1999).
17. Wolpaw, A.J. *et al.* Modulatory profiling identifies mechanisms of small molecule-induced cell death. *Proc. Natl. Acad. Sci. USA* **108**, E771–E780 (2011).
18. Degterev, A. *et al.* Chemical inhibitor of nonapoptotic cell death with therapeutic potential for ischemic brain injury. *Nat. Chem. Biol.* **1**, 112–119 (2005).
19. Takahashi, N. *et al.* Necrostatin-1 analogues: critical issues on the specificity, activity and in vivo use in experimental disease models. *Cell Death Dis.* **3**, e437 (2012).
20. Yang, W.S. & Stockwell, B.R. Synthetic lethal screening identifies compounds activating iron-dependent, nonapoptotic cell death in oncogenic-RAS-harboring cancer cells. *Chem. Biol.* **15**, 234–245 (2008).
21. Shoemaker, R.H. The NCI60 human tumour cell line anticancer drug screen. *Nat. Rev. Cancer* **6**, 813–823 (2006).
22. Shimada, K., Hayano, M., Pagano, N.C. & Stockwell, B.R. Cell-line selectivity improves the predictive power of pharmacogenomic analyses and helps identify NADPH as biomarker for ferroptosis sensitivity. *Cell Chem. Biol.* **23**, 225–235 (2016).
23. Romanowska, M. *et al.* Effects of selenium supplementation on expression of glutathione peroxidase isoforms in cultured human lung adenocarcinoma cell lines. *Lung Cancer* **55**, 35–42 (2007).
24. Fradejas, N. *et al.* Mammalian Trit1 is a tRNA([Ser]Sec)-isopentenyl transferase required for full selenoprotein expression. *Biochem. J.* **450**, 427–432 (2013).
25. Song, J.H. *et al.* Deletion of Pim kinases elevates the cellular levels of reactive oxygen species and sensitizes to K-Ras-induced cell killing. *Oncogene* **34**, 3728–3736 (2015).
26. Tansey, T.R. & Shechter, I. Structure and regulation of mammalian squalene synthase. *Biochim. Biophys. Acta* **1529**, 49–62 (2000).
27. Liu, C.-I. *et al.* Structural insights into the catalytic mechanism of human squalene synthase. *Acta Crystallogr. D Biol. Crystallogr.* **70**, 231–241 (2014).
28. Chugh, A., Ray, A. & Gupta, J.B. Squalene epoxidase as hypocholesterolemic drug target revisited. *Prog. Lipid Res.* **42**, 37–50 (2003).
29. Gueven, N., Woolley, K. & Smith, J. Border between natural product and drug: comparison of the related benzoquinones idebenone and coenzyme Q_{10}. *Redox Biol.* **4**, 289–295 (2015).
30. Dixon, S.J. *et al.* Human haploid cell genetics reveals roles for lipid metabolism genes in nonapoptotic cell death. *ACS Chem. Biol.* **10**, 1604–1609 (2015).
31. Hirsch, H.A. *et al.* A transcriptional signature and common gene networks link cancer with lipid metabolism and diverse human diseases. *Cancer Cell* **17**, 348–361 (2010).
32. Santos, C.R. & Schulze, A. Lipid metabolism in cancer. *FEBS J.* **279**, 2610–2623 (2012).
33. Kamphorst, J.J., Fan, J., Lu, W., White, E. & Rabinowitz, J.D. Liquid chromatography-high resolution mass spectrometry analysis of fatty acid metabolism. *Anal. Chem.* **83**, 9114–9122 (2011).

Acknowledgments

We thank H. Li (Columbia University, New York, New York, USA) and C. Henderson (Biogen Idec, Cambridge, Massachusetts, USA) for providing mevalonic acid and farnesyl pyrophosphate, C.-I. Liu and A.H.J. Wang (Academia Sinica, Taipei, Taiwan) for the truncated human squalene synthase construct, R. Weinberg (Whitehead Institute, Cambridge, Massachusetts, USA) for engineered BJ cell lines (BJeLR, DRD, BJeHLT, and BJeH), E. Schon (Columbia University, New York, New York, USA) for 143B cells, E. Lee for assistance with ACC experiments, and V. Viswanathan for helpful discussions. This research was funded by the Howard Hughes Medical Institute, the US National Institutes of Health (grants 5R01CA097061, 5R01GM085081, and R01CA161061 to B.R.S.), New York Stem Cell Science (grant C026715 to B.R.S.) and the US National Cancer Institute (K99 Pathway to Independence Award 1K99CA166517-01 to S.J.D.).

Author contributions

K.S. and B.R.S. conceived of the project, designed the experiments, analyzed the data, and wrote the manuscript. K.S. performed all experiments and analyses except the following: R.S. and C.A.V. synthesized CIL56 analogs; A.K. expressed and purified SQS protein and performed confirmatory SQS pulldown experiments and competition assays; W.S.Y. performed the GPX4 enzymatic assay; and M.H. performed confirmatory siRNA experiments. L.M.B. performed proteomic analysis for target identification. S.J.D. participated in characterization of TOFA's effect on FIN56. A.J.W. assisted in modulatory profiling experiments. S.J.D. assisted in writing the manuscript.

Competing financial interests

The authors declare no competing financial interests.

Additional information

Any supplementary information, chemical compound information and source data are available in the online version of the paper. Reprints and permissions information is available online at http://www.nature.com/reprints/index.html. Correspondence and requests for materials should be addressed to B.R.S.

ONLINE METHODS

Chemicals. We purchased 3,169 uncharacterized lethal compounds, as well as structural analogs of CIL41/70, from Asinex, ChemBridge, ChemDiv, Enamine, InterBioScreen, MayBridge, TimTec, Vitas M Labs, and Zelinsky. Chemical modulators (**Supplementary Table 2**) used in modulatory profiling were obtained as described[17]. U0126 was obtained from LC Laboratories. Deferoxamine mesylate, α-tocopherol, sodium selenite, zaragozic acid A, mevalonolactone and simvastatin were purchased from Sigma-Aldrich. Cerivastatin was obtained from Waterstone Technology. Lovastatin was obtained from Santa Cruz Biotechnology. YM-53601 and TOFA were purchased from Cayman Chemical. Isoprenoid pyrophosphate (isopentenyl-PP, dimethylallyl-PP, geranyl-PP, farnesyl-PP and geranylgeranyl-PP) ammonium salts were purchased from Isoprenoids. Idebenone was purchased from Tocris Bioscience. Pim kinase inhibitors (CX-6258 and AZD-1208) were purchased from Selleck Chemicals. Erastin and (*1S*,*3R*)-RSL3 were synthesized as described previously[12,34]. NB-598 maleate was purchased from ChemScene. CIL56, FIN56, and their structural analogs were synthesized as described[35] (#WO2008140792A1). Building blocks for these compounds were purchased from Matrix Scientific and Sigma-Aldrich. The purity of the purchased compounds was not assessed. Structures of 56 CILs and CIL41/70 analogs are presented in **Supplementary Note 1**. The total synthesis of CIL56 analogs and their ^{1}H NMR data are described in **Supplementary Note 2**.

Cell lines and media. Four engineered BJ cell lines (BJeLR, DRD, BJeHLT, and BJeH) were obtained from Robert Weinberg (Whitehead Institute). 143B cells (osteosarcoma) were from Eric Schon (Columbia University). Calu-1 (lung adenocarcinoma) and HT-1080 (fibrosarcoma) cells were from American Type Culture Collection. The four BJ cell lines were grown in DMEM high-glucose media (Life Technologies), 20% Medium 199 (Sigma), and 15% heat-inactivated FBS (FBS). HT-1080 cells were grown in DMEM high-glucose media with 1% non-essential amino acids (Life Technologies) and 10% FBS. 143B cells were grown in DMEM high-glucose media with 1% glutamine and 10% FBS. Calu-1 cells were grown in McCoy's 5A media (Life Technologies) supplemented with 10% FBS. All the cell lines were grown at 37 °C under 5% CO_2. Cell lines were not tested for mycoplasma.

Cell viability assay. We seeded 1,000 cells per 36 μl in each well in 384-well plates. Lethal compounds were dissolved, and a twofold, 12-point dilution series was prepared in DMSO. Compound solutions were further diluted with media at 1:25, and 4 μl per well of the diluted solutions was added to cell cultures immediately after cells were seeded. When ferroptosis inhibitors (100 μM α-tocopherol, 152 μM deferoxamine, or 10 μM U0126) were used in cotreatments with lethal inducers, they were supplemented to cell culture when the lethal compounds were added, and the cells were then incubated for 24 h. When other cell-death-modulating compounds (100 nM sodium selenite, 1 μM cerivastatin, 100 μg/mL mevalonic acid) were used in cotreatments, they were supplemented to cell culture for 24 h before lethal compounds were added to cell culture, after which cells were further incubated for 24 h at 37 °C under 5% CO_2. On the day of the viability measurement, we added 10 μl per well of 50% Alamar Blue diluted in media (Life Technologies) and further incubated the cells at 37 °C for 6 h. Fluorescence intensity (excitation/emission: 530/590) was measured with a Victor 3 plate reader (PerkinElmer), and the normalized viability was calculated as $V_L = (I_L - I_0)/(I_V - I_0)$, where V_L, I_0, I_V, and I_L are the normalized viability and the raw fluorescence intensities from the wells containing media, cells treated with a vehicle (negative control), and cells with the lethal compound (L), respectively. When the effect of a chemical modulator (M) on L was calculated, we instead used the equation $V_{L|M} = (I_{M,L} - I_0)/(I_{M,V} - I_0)$, where $V_{L|M}$, $I_{M,L}$ and $I_{M,V}$ are the normalized viability, and fluorescence intensity from cells treated with M and V, and from cells with M and L, respectively. The viability was typically measured in biological triplicate unless otherwise specified. A representative dose-response curve, the mean and standard error of normalized viability from one replicate were plotted. HT-1080 viability after modulator treatments corresponding to **Figures 3c** and **5e**,**f** is available in **Supplementary Figure 13a–c**.

Caspase-3/7 activation assay. The Apo-ONE Homogeneous Caspase-3/7 Assay (Promega) was used according to the manufacturer's protocol, with a minor modification. First, we optimized the assay (**Supplementary Fig. 1a**,**b**). HT-1080 cells were seeded at 1,000 cells per 40 μl in each well of a 384-well plate, incubated for 1 h, and treated with test compounds for different durations (from 3.5 to 48 h). 15 μl of culture media was aspirated from each well, and 5 μl of a mixture of lysis buffer and caspase-3/7 fluorogenic substrate from the kit was added. Plates were kept in the dark at room temperature for 16 h, and the fluorescence (excitation/emission: 490/535) of each well was measured using a Victor 3 plate reader. In the optimization, the fluorescence of apoptosis-inducer-treated cells started increasing after 6–12 h, and lethal compounds that induced strong positive signals in the end (i.e., apoptosis inducers) were distinguished from non-apoptotic inducers as early as after 18 h. We therefore treated cells with lethal compounds for 18 h in further analyses. In the screening mode, we incubated HT-1080 cells with screening molecules for 18 h, processed cells, and measured the fluorescence. Compounds inducing fluorescence with similar intensity as vehicle (DMSO) treatments were defined as caspase-independent lethals.

Discovery of novel ferroptosis inducers using modulatory profiling. *Collection of CILs.* We first collected uncharacterized synthetic compounds from various vendors for different screening purposes. Of those, we found 3,169 compounds to be lethal in BJeLR cells. We first sought compounds that induced non-apoptotic cell death in two ferroptosis-susceptible cell lines, HT-1080 and BJeLR. We tested the 3,169 compounds at 5.3 μg/mL in those two cell lines, and 451 compounds showed (i) an EC_{80} < 2.8 μg/mL in both cell lines and (ii) no activation of caspase-3/7 at 5.3 μg/mL. Cell viability and caspase-3/7 activity assays were performed as described above. The 95th percentile of Apo-ONE fluorescence from 0.13% DMSO-treated cells was set as the threshold of caspase-independent lethality, and the raw fluorescent value of each well was divided by the threshold for normalization; lethal compounds were considered caspase-3/7-independent when the normalized fluorescent values were less than one. These compounds were defined as CILs. Next, we computed the structural similarity among the 451 compounds based on Pubchem's fingerprint[36] and removed structurally similar compounds (cutoff: Tanimoto coefficient of 0.9). We also removed compounds that did not satisfy Lipinski's rule of five with a minor modification (no more than five hydrogen bond donors, no more than ten hydrogen bond acceptors, molecular weight ranging from 250 to 500, a partition coefficient log P not greater than five) and compounds whose biological activities were known. Finally, we retested the selected compounds in twofold dilution series in the two cell lines and closely examined 56 compounds with low EC_{50} in modulatory profiling.

Modulatory profiling of CILs. We examined 56 CILs using modulatory profiling[17] (**Supplementary Fig. 2**). HT-1080 and BJeLR cells were seeded at 1,000 cells per 40 μl in each well of a 384-well plate. They were cotreated with a lethal compound (L) and a death modulator (M) in technical triplicates. We added 56 CILs to cells in a twofold, 14-point dilution series. Death modulators were reagents known to perturb cell death signaling pathways and were treated at a single concentration, as described previously[17]. Cells were incubated with lethal compounds and modulators for 48 h, and the normalized viability was measured as described above. For each combination of L and M, the area under the dose-response curve (AUC) was computed. An effect of M on L ($E_{M|L}$) was represented by the difference in AUCs between the modulator ($AUC_{M,L}$) and the vehicle ($AUC_{V,L}$), or $E_{M|L} = AUC_{M,L} - AUC_{V,L}$ (**Supplementary Fig. 2b**). When M suppresses or enhances the effect of L, $E_{M|L} > 0$ or $E_{M|L} < 0$, respectively.

The modulatability of each L (m_L) was an average of the absolute value of the effect of all M's on L, or $m_L = \sum_M |E_{M|L}|/n_M$, where n_M is the number of modulators, 46. Large m_L indicates that L induces a selective cell death phenotype[17]. We computed m_L for each CIL and each known lethal compound from different classes of mechanism of action (i.e., HDAC inhibitors, proteosomal inhibitors, mitochondrial uncouplers, topoisomerase I and II inhibitors, microtubule destabilizers, and ferroptosis inducers). m_L of CILs larger than the median value of known lethal compounds' m_L were considered 'high'; we identified high-modulatability CILs. For generating hierarchical clustering of the modulatory profiles, the distance between modulatory profiles (P) of two compounds P_i and P_j was defined by $d_{ij} = 1 - \mathrm{Corr}_{\mathrm{Pearson}}(P_i,P_j)$, and hierarchical clustering with an average-linkage method was used to generate dendrograms.

doi:10.1038/nchembio.2079

Cobalt (II) binding assay *in vitro*. For each cluster I compound (CIL13, -52, and -64), we prepared twofold dilution series with DMSO. We added 30 µL per well of either water or 10 µM cobalt (II) chloride solution to each well of a 384-well plate. Dilution series of each compound in DMSO were added by 10 µL per well. After solutions had been mixed by shaking of the plate using a Victor 3 plate reader (PerkinElmer), absorbance was scanned between 300 and 700 nm for each compound. Finally the following Absorbance value for each compound was plotted (**Supplementary Fig. 3b**):

$$\begin{aligned}\Delta\Delta\text{Absorbance} &= \Delta\text{Abs}_{\text{CIL,Co2+}} - \Delta\text{Abs}_{\text{CIL,water}} \\ &= (\text{Abs}_{\text{CIL,Co2+}} - \text{Abs}_{\text{DMSO,Co2+}}) - (\text{Abs}_{\text{CIL,water}} - \text{Abs}_{\text{DMSO,water}})\end{aligned}$$

where Abs is the absorbance at each wavelength.

Search of commercially available structural analogs of CIL41/70. Structural analogs possessing the core scaffold of CIL41/70 (SMILES: C(= O)([*])O/*N* = C([*])/N) were searched for in eMolecules (http://www.emolecules.com) and purchased from the vendors listed above. Their lethality was tested once in HT-1080 cells in technical triplicates.

Analysis of ROS generation. We grew 200,000 HT-1080 or BJeLR cells in six-well plates at 37 °C for 16 h. Cells were treated with test compounds, trypsinized, pelleted, and washed once with PBS. For lipophilic or aqueous ROS detection, cells were re-suspended in Hanks' Balanced Salt Solution (HBSS; Life Technologies) containing test compounds as well as C_{11}-BODIPY(581/591) (2 µM) or H_2-DCFDA (25 µM), respectively (Life Technologies), and incubated for 10 min at 37 °C. Cells were then pelleted, re-suspended in 500 µL HBSS, strained through a 40-µm cell strainer (BD Falcon), and analyzed using a BD Accuri C6 flow cytometer (BD Biosciences). Both dyes were measured in the FL1 channel. Experiments were done in biological triplicates.

Glutathione-quantification assay. We seeded 500,000 HT-1080 cells in a 10-cm dish. Cells were grown at 37 °C for 16 h. On the day of the analysis, cells were cotreated with 100 µM α-tocopherol and either vehicle (DMSO) or a ferroptosis inducer (10 µM erastin, 0.5 µM (*1S*,*3R*)-RSL3, or 5 µM FIN56) and incubated for 10 h. Cells were then trypsinized, pelleted, washed once with 400 µL of ice-cold PBS containing 1 mM EDTA, and sonicated. After the cell debris had been pelleted and removed, both oxidized and reduced glutathione in 120 µL of sample was quantified in technical triplicates using the QuantiChrome glutathione assay kit (BioAssay Systems). The glutathione quantity was normalized to the protein concentration measured via Bradford assay (Bio-Rad).

GPX4 enzymatic activity assay. We seeded 17 million BJeLR cells in 225-cm^2 tissue culture flasks (Corning). We then added vehicle (0.1% DMSO for 11 h) or test compound (10 µM erastin for 11 h, 0.5 µM (*1S*,*3R*)-RSL3 for 2 h, or 5 µM FIN56 for 10 h). The GPX4 enzymatic activity assay was performed as described previously[12]. Briefly, 10 million cells were resuspended in cell lysis buffer. Cells were sonicated to make cell lysates that were then cleared by centrifugation at 14,000 r.p.m. for 10 min. The protein concentration of the cleared cell lysates was determined via Bradford protein assay. We mixed 200 µg of cellular protein with phosphatidyl choline hydroperoxide, a GPX4-specific substrate, and reduced glutathione, a GPX4 cofactor. The mixture was incubated at 37 °C for 30 min and then subjected to lipid extraction using chloroform:methanol (2:1) solution. The lipid extract was evaporated using a Rotavap and re-dissolved in 100% ethanol before being injected into the LC-MS instrument for 2-linoleoyl-1-palmitoyl-*sn*-glycero-3-phosphocholine (PLPC) quantitation.

Reverse-transcription quantitative PCR. We trypsinized 0.2 to 1 million cells grown in six-well dishes, pelleted them, resuspended them in Buffer RLT (Qiagen), and homogenized them with QIAshredder (Qiagen). RNA was further extracted using the RNeasy Mini Kit (Qiagen). We converted 2 µg of extracted RNA from each sample into cDNA using TaqMan reverse-transcription reagents (Life Technologies). qPCR primers were designed to detect all splicing variants using Primer Express 2.0 (Applied Biosystems). The designed primers were confirmed to amplify only the designated gene transcripts using *in silico* PCR (http://genome.ucsc.edu/cgi-bin/hgPcr). For qPCR reactions, primers, cDNA, and Power SYBR Green PCR Master Mix (Applied Biosystems) were mixed, and quantitation was performed using a StepOnePlus real-time PCR system (Applied Biosystems). Experiments were done in biological triplicates.

Western blotting. We seeded 300,000 cells (HT-1080 or BJeLR) per well in six-well plates. For cotreatment, ferroptosis inducers (10 µM erastin for 11 h, 0.5 µM (*1S*, *3R*)-RSL3 for 2 h, or 5 µM FIN56) and 100 µM α-tocopherol were added to cell culture at the same time, and cells were then incubated for 10 h (**Fig. 2e**). When other death-modulating compounds (100 nM sodium selenite, 1 µM cerivastatin, 100 µg/mL mevalonic acid, 30 µM C75, or 2 µM cerulenin) were used in cotreatments, cells were pre-incubated with the modulators for 24 h before being treated with ferroptosis inducers for 6 h. Cell lysis, SDS–PAGE and protein transfer to PVDF membrane were performed as previously described[9]. We used the following antibodies: anti-human α-tubulin (Santa Cruz Biotechnology, sc-32293, 1:10,000 dilution), anti-human GPX4 (Abcam, ab41787, 1:2,000 dilution), anti-human GPX1 (R&D Systems, AF3798, 1:1,000 dilution), and anti-human SQS (Abcam, ab109723 for full-length, ab195046 for truncated, both at 1:1,000 dilution). Secondary antibodies were from LI-COR (1:3,000 dilution). The PVDF membranes labeled with primary and secondary antibodies were scanned using an Odyssey Imaging System (LI-COR). Experiments were performed in biological triplicates, and the mean ± s.e. of intensity was plotted. Full gel images are shown in **Supplementary Figure 14**.

Gene-knockdown experiment. shRNAs designed by the RNAi Consortium were used, and gene knockdown was performed as described previously[9]. For siRNA-mediated gene-knockdown experiments, HT-1080 cells were reverse-transfected with 5 nM siRNA. siRNA targeting *GPX4* (Dharmacon, #L-011676-00) or *TRIT1* (Dharmacon, #L-018831-02) or nontargeting siRNA (Qiagen) was mixed with 2 µL Lipofectamine RNAiMAX (Invitrogen) in a well of a 12-well plate. After incubation for 30 min at room temperature, 30,000 cells were added to each well, and knockdown was allowed to proceed for 48 h. Cells were then harvested and re-seeded for RT-qPCR, viability assay, and western blotting. For RT-qPCR, cells were re-seeded into 12 well plates and harvested the following day as described above. For viability assay, 1,000 cells per well were re-seeded into 384-well plates for 24 h and were then incubated with compounds for another 24 h before the addition of Alamar Blue. Compounds were added in a 12-point twofold dilution series, with the highest concentrations of compound being 36.5 µM (erastin), 10 µM ((*1S*,*3R*)-RSL3), and 38.7 µM (FIN56). For western blotting, cells were harvested 48 h after knockdown (no re-seeding).

FIN56 target identification. *Conjugation of active and inactive probes with Profinity epoxide resin.* We incubated 6 µmol of active (SRS11-31) or inactive (SRS11-66) probes dissolved in 500 µL DMSO and 300 mg of Profinity epoxide resin (Bio-Rad) in saturated sodium bicarbonate at 45 °C for 3 d. We ended the conjugation reaction by adding 120 µL of 1 M ethanolamine to the reaction mixture. The conjugated probe beads were used for further protein pulldown assay.

Affinity chromatography with active and inactive probe beads. We seeded 8 million HT-1080 cells in two 15-cm polystyrene tissue culture dishes and allowed the cells to grow overnight. Culture media was removed from dishes, and cells were washed five times with cold PBS. After the PBS had been completely removed, the cells were treated with 2 mL of lysis buffer (25 mM MOPS (pH 7.2), 15 mM EGTA, 15 mM $MgCl_2$, 2 mM DTT, 1 mM sodium orthovanadate, 1 mM sodium fluoride, 0.5% NP-40, 60 mM β-glycerophosphate, protease inhibitor cocktail (Sigma-Aldrich P8340)) per plate, scraped, and collected. Cells were then agitated at 4 °C for 15 min, after which insoluble components were precipitated at 14,000*g* at 4 °C for 10 min, the supernatant was removed, and the protein concentration was measured via Bradford assay.

We incubated 250 µg of protein (up to 400 µL of the whole-cell lysate) with active and inactive probe beads, added 20 mL of bead buffer (50 mM Tris-HCl (pH 7.4), 250 mM NaCl, 5 mM EDTA, 5 mM EGTA, 5 mM NaF, 0.1% NP-40), and incubated the mixture at 4 °C for 12 h. Beads were then collected using Poly-prep chromatography columns (Bio-Rad). Beads were then washed with 8 mL of bead buffer three times and transferred to Eppendorf tubes.

Bacterial expression and purification of truncated human SQS for competition assay. The plasmid encoding the truncated human squalene synthase

(SQS 31-370) in pET28a expression vector, kindly provided by Chia-I Liu and Andrew H.J. Wang (Academia Sinica, Taiwan), was confirmed by DNA sequencing (Gene Wiz, Inc.) and then used to transform *Escherichia coli* BL21-Gold (DE3) competent cells (Agilent Technologies). The cells with the construct were grown in LB media supplemented with 100 µg/mL ampicillin at 37 °C until the OD_{600} reached 1. Protein expression was induced with 0.5 mM isopropyl β-D-thiogalactoside at 17 °C overnight (12–13 h). Cells were pelleted (4,000*g*, 20 min, 4 °C) and lysed by sonication in SQS buffer (50 mM Tris, pH 7.4, 250 mM NaCl, 5 mM imidazole, 5 mM $MgCl_2$, 1 mM TCEP). Cell lysate was then centrifuged at 15,000*g* for 45 min at 4 °C. The supernatant was loaded onto a chromatography column containing Ni Sepharose 6 Fast Flow beads (GE Life Sciences) equilibrated with SQS buffer. After two washes and one nonspecific wash of the beads, the bound SQS was eluted with 250 mM i midazole in the same buffer. The purity of eluted fractions was verified by SDS–PAGE as more than 90% pure. The fractions containing SQS were concentrated, flash-frozen, and stored at −80 °C. Protein concentration was determined using absorbance at 280 nm with a molar extinction coefficient (ε) of 42,860 M^{-1} cm^{-1} (for reduced SQS with an N-terminal His_{12} tag as calculated from the amino acid sequence by ExPASy ProtParam).

SQS competition assay with purified truncated SQS, FIN56, and active probe. Purified truncated SQS was prepared as described above. The protein solution was diluted with bead buffer (50 mM Tris-HCl, pH 7.4, 250 mM NaCl, 5 mM EDTA, 5 mM EGTA, 5 mM NaF, 0.1% NP-40, 1 mM TCEP). We mixed 190 µL of 1 or 10 ng/mL SQS solution with 10 µL of DMSO or competitor solution (2 mM FIN56 solution in DMSO), with DMSO and FIN56 at final concentrations of 5% and 100 µM, respectively. This mixture was rotated and incubated at 4 °C for 2 h. We added 15 µL of active probe-bead solution (33% slurry) to the solution and incubated it for another 2 h. The beads were spun down (500 r.p.m., 4 °C, 1 min), and supernatant was removed and washed with 500 µL of bead buffer three times. After the third wash, 20 µL of 3× SDS sample loading buffer was added, and the mixture was boiled at 95 °C for 5 min. Samples were spun for 1 min at 13,000 r.p.m. in a table-top centrifuge, and 10 µL of each sample was loaded on gels for SDS–PAGE. SQS was confirmed by immunoblotting.

Proteomic analysis for target identification. At Quantitative Proteomics Center at Columbia University, the proteins in pulldown samples with active (SRS11-31) and inactive (SRS11-66) beads were eluted at 80 °C in 50 mM ammonium bicarbonate with 0.1% Rapigest detergent with protease inhibitor cocktail P8340 (Sigma-Aldrich). Biological triplicate culture and affinity pulldowns for bound active and inactive compound were prepared. Cysteines in the protein samples were reduced with dithiothreitol and alkylated with iodoacetamide, and proteins were digested with trypsin (6 ng/µL, Promega Corp, #V511A, in 50 mM ammonium bicarbonate). A digest of yeast alcohol dehydrogenase (50 fmol) was added as an internal detection control.

Three chromatograms were recorded for each of six biological replicates (three active, three inactive), yielding 12 chromatograms. Analytical separation was done on a NanoAcquity UPLC (Waters), with a 120-min chromatogram on a 75-µm inner diameter × 25-cm HSS T3 1.8-µm-particle-diameter reverse-phase C18 column at a flow rate of 300 nL/min with an acetonitrile/formic acid gradient at 45 °C. Identification and quantitation of proteins bound to the beads was done by label-free proteomic profiling on a Synapt G2 HDMS (quadrupole-time-of-flight) mass spectrometer (Waters) using data-independent scanning (MS^E) as described previously[12], except that spectra were recorded in positive-ion sensitivity mode without ion mobility. Spectra were searched against a human UniProt complete proteome with ProteinLynx Global Server version 2.5 RC9 (Waters) and post-processed with Elucidator software version 3.3.0.1.SP3_CRE52.21 (Ceiba Solutions, Inc.) as described previously[37].

Target validation using custom shRNA library. Custom lentiviral shRNA libraries were generated using plasmids encoding the first generation of the RNAi Consortium shRNAs targeting 70 genes identified by chemoproteomics according to the RNAi Consortium's instructions. These lentiviral shRNAs were laid out in an arrayed format using 384-well plates and were infected in four cell lines (HT-1080, BJeLR, Calu-1, and 143B). Our rationale for the screening design was that if shRNAs target the *bona fide* FIN56 targets, those shRNAs should show 'consistent' FIN56-enhancing or -suppressing effects in all four cell lines, depending on how FIN56 acts on the target protein (**Supplementary Fig. 8a**). If the shRNAs act on off-targets to change sensitivity to FIN56, their effects should be less consistent. Gene knockdown was performed as described above; 400 cells per well in 384-well plates were seeded and incubated for a day, lentivirus-containing shRNAs were infected in them on the next day, and puromycin was added 2 d after infection. Cells were treated with twofold eight-point dilution series of FIN56 after 24 h and incubated for another 48 h before Alamar Blue was added, after which the cells were incubated for 6 h.

Data analysis for discovering functionally relevant targets. Alamar Blue fluorescence intensity data were normalized as described above. For each cell line, dose-response curves for FIN56 for each shRNA treatment were plotted and overlaid on a single plot first. From among eight tested concentrations of FIN56, extreme (low or high) concentrations that did not kill or completely kill cells treated with any shRNAs were removed; eventually four or five more informative concentrations were used for further analysis, as in **Figure 4b** and **Supplementary Figure 8b**. For each shRNA treatment, the AUC after FIN56 treatment in dilution series was computed and rank-ordered across all tested shRNAs in each cell line. Based on their 'consistency' across four cell lines and the magnitude of effects, shRNAs were classified into 11 categories (5 consistently suppressing groups (top 10%, top 20%, etc.), 5 consistently enhancing groups (top 10%, etc.), and nonconsistent). Note that 'nonconsistent' indicates that the shRNA induced FIN56-enhancing effects in some cell lines and FIN56-suppressing effects in others. A gene was ranked according to the consistent effects of shRNAs targeting it. When at least one of the shRNAs targeting a gene showed consistent FIN56-enhancing or -suppressing effects, the gene was considered a potentially functionally relevant target of FIN56, through loss-of-function or gain-of-function scenarios, respectively.

Validation of loss-of-function targets using pooled siRNAs. Candidate loss-of-function targets of FIN56 were further targeted by pooled siRNAs. Previously, pooled siRNA against GPX4, a target of RSL3, was shown to phenocopy RSL3; siGPX4 induced ferroptosis that was suppressed by α-tocopherol as well as oncogenic Ras selectivity across BJ series. Expecting that siRNAs against *bona fide* loss-of-function targets would induce ferroptosis, we treated siRNAs against the candidates as well as GPX4 as a positive control. siRNAs were transfected into BJeLR cells. We incubated 1 mL of Opti-MEM (Life Technologies) mixed with 20 pmol of pooled siRNA and 5 µL of RNAiMAX (Life Technologies) to form a complex for 15 min, and we then aliquoted 500 µL per well into six-well dishes. Next, 120,000 BJeLR cells per 1.5 mL in each well were seeded and grown for 2 d. Cells were then trypsinized and seeded again at 120,000 per well and grown with or without supplementation of α-tocopherol. After 2 d, cells were trypsinized and cell density was measured using an automated cell counter (Vicell, Beckman Coulter).

Statistical analysis and data visualization. Dose-response curve plotting and EC_{50} computation were done with Prism 5.0c. *P* values for the differences in EC_{50} values were computed on the basis of model comparison with Akaike's information criterion. The rest of the statistics and plotting were done using R language and the following R packages and functions: ChemmineR package for Pubchem's fingerprint and Tanimoto coefficient computation, heatmap.2 function in the gplots package for plotting heat maps, and flowCore and flowViz packages modified for plotting .fcs files in flow cytometry. The statistical significance of protein expression (on western blots) was calculated using paired two-tailed *t*-tests.

34. Yagoda, N. *et al.* RAS-RAF-MEK-dependent oxidative cell death involving voltage-dependent anion channels. *Nature* **447**, 864–868 (2007).
35. Cholody, W.M. *et al.* Derivatives of fluorene, anthracene, xanthene, dibenzosuberone and acridine and uses thereof. US patent application PCT/US2008/006015 (2008).
36. Backman, T.W.H., Cao, Y. & Girke, T. ChemMine tools: an online service for analyzing and clustering small molecules. *Nucleic Acids Res.* **39**, W486–W491 (2011).
37. Alegre-Aguarón, E. *et al.* Growth factor priming differentially modulates components of the extracellular matrix proteome in chondrocytes and synovium-derived stem cells. *PLoS One* **9**, e88053 (2014).

doi:10.1038/nchembio.2079